Liquid to Hexatic to Crystalline Order in Langmuir-Blodgett Films

Ravishankar Viswanathan,* Lars L. Madsen, Joseph A. Zasadzinski,† Daniel K. Schwartz

Atomic force microscope images of zinc arachidate (ZnA_2) Langmuir-Blodgett films show that three- and five-layer films are "hexatic," with long-range bond-orientational order and short-range positional correlations of three to five lattice repeats. The monolayer in contact with the substrate is disordered. Films of seven or more layers of ZnA_2 are crystalline. A population of dislocations, most likely originating at the substrate, disrupts the positional but not the orientational order of the lattice, leading to hexatic layers intermediate between crystal and liquid. The influence of the substrate propagates farther into ZnA_2 films than into cadmium arachidate films because the molecular cohesion is much weaker in ZnA_2 than in cadmium arachidate, as evidenced by a less dense molecular packing.

Substrate effects play an important but poorly understood role in determining the evolution of in-plane ordering of Langmuir-Blodgett (LB) films. Although thick LB films of fatty acid salts are similar to their bulk crystals, proximity to the substrate leads to various levels of disorder in thinner films, depending on the physical and chemical nature of the substrate and the film (*1*). Infrared spectroscopy and electron diffraction also suggest that the structure of LB films evolves toward that of thick films as the number of layers increases (*2*). In practice, a number of buffer layers are used to eliminate substrate effects on ordering in LB film applications. Atomic force microscope (AFM) studies have shown that for fatty acid salts on atomically smooth crystalline mica or amorphous oxidized Si [with the exceptions of Pb and Mn salts on mica (*3*)], monolayer films are disordered and have a liquid-like structure (*1*, *4*). The "bulk" crystal structure for Cd, Mn, Ba, Ca, and Mg fatty acid salts appears immediately after deposition of an additional bilayer to form a trilayer (*1*, *4*).

However, in ZnA_2 films, an intermediate hexatic structure appears between the liquid-like monolayer and the crystalline thick films. The in-plane molecular organization of ZnA_2 films is also unique; the alkane chains of ZnA_2 films are packed in a hexagonal lattice with a nearest neighbor spacing of 0.48 nm tilted 30° toward nearest neighbors, resulting in an interfacial area per molecule of 0.22 nm^2 [20% greater than the area for CdA_2 (*1*)]. The symmetry and density of the in-plane lattice do not change with the number of layers, but the extent of positional and orientational order increases with an increasing number of layers. The lattice is similar to the R2 rotator phase found in bulk saturated alkanes near their melting point, although in the alkanes the R2 phase is untilted (*5*, *6*). This packing is unusual because (i) the hexagonal lattice shows that the molecules have lost the elliptical shape and all-*trans* configuration usually associated with crystalline order in saturated alkanes, and (ii) the molecules are less densely packed than in either the herringbone or triclinic structures common to the other fatty acid salts. This more open lattice structure suggests that the in-plane cohesion is much less in ZnA_2 than in CdA_2. This lack of in-plane cohesion allows the disordering effect of the substrate to propagate farther into ZnA_2 films than into CdA_2 films, resulting in a hexatic organization with long-range orientational and short-range translational order for films with a number of layers intermediate between the liquid monolayer and the multilayer crystalline thick films.

Resolving the structure of LB films at sufficient resolution to determine positional and orientational order is only possible with the AFM (*7*). For LB films, lattice spacings and symmetries (*1*, *3*, *4*, *8*) and molecular defects such as elementary dislocations and grain boundaries (*1*, *9*, *10*) can be resolved with an AFM even if applied forces as large as 10^{-8} N are used (*11*). In this study, seven types of ZnA_2 LB films were examined: films of one, three, five, seven, and nine layers on mica, and films of three and seven layers on amorphous oxidized Si (*12*). AFM measurements were performed at ambient temperature with a Nanoscope III (Digital Instruments, Santa Barbara, California) with a 1 μm by 1 μm scan head and a silicon nitride tip on a cantilever with a spring constant of 0.12 N/m. The best molecular resolution was achieved in the "force mode," in which the tip is scanned at constant height and spring deflection is measured (*13*). We found no quantitative differences between the films deposited on mica or Si substrates, which indicates that the hexagonal ordering of the films is not due to epitaxial growth on the ordered mica substrate (*3*). Instead, the substrate provides a break in the normal bilayer symmetry and an anchoring point with which to begin the layer sequence. Monolayer films of ZnA_2 show only a featureless flat surface with no molecular ordering, similar to that in monolayers of CdA_2 and other fatty acid films that we have interpreted as liquid-like ordering (*1*).

An AFM image of a seven-layer film of ZnA_2 on mica shows an absence of lattice defects and the presence of regular crystalline order (Fig. 1A). The sharp, symmetric reflections in the two-dimensional (2D) Fourier transform (FT) confirm that both the positional and orientational order are long-range (Fig. 1B). Similar images were obtained for all ZnA_2 films of seven or more layers on both mica and oxidized Si substrates. The six strongest reflections in the FT form a distorted hexagonal pattern with two distinct lattice repeats of 0.483 ± 0.006 nm by 0.557 ± 0.006 nm, with an angle of 54.7° ± 0.5° between them. The resulting interfacial area per molecule is 0.219 ± 0.008 nm^2. From the lattice repeats and the measured bilayer thickness of 4.7 ± 0.2 nm, we propose that the molecular packing in the plane perpendicular to the long axis of the fatty acid molecules is hexagonal and that the molecules are tilted toward nearest neighbors at an angle of 30° ± 2° (*14*). This tilted hexagonal lattice is unusual; in every other LB film of fatty acid salts that we examined, the lattice is based on either herringbone or triclinic patterns that maximize the close packing of the elliptical-shaped, all-*trans* alkane molecule (*15*). A hexagonal packing with a nearest neighbor spacing of 0.48 nm is similar to the R2 rotator phase in bulk saturated alkanes (*5*, *6*). In the rotator phases, the alkane chains have much freer rotation about their long axes and the molecules have a more cylindrical symmetry than in ordinary crystalline phases. However, in the alkane R2 phase, the molecules are untilted; the additional constraint of interfacial density imposed by the counterion leads to a new lattice structure. From the measured interfacial density and tilt, the cross-sectional area perpendicular to the chains in ZnA_2 is ≈19 $Å^2$, a 5 to 6% lower density than in CdA_2 in which the chains adopt a more closely packed herringbone lattice (*1*).

R. Viswanathan, L. L. Madsen, J. A. Zasadzinski, Department of Chemical Engineering, University of California, Santa Barbara, CA 93106, USA.
D. K. Schwartz, Department of Chemistry, Tulane University, New Orleans, LA 70118, USA.

*Present address: Raychem Corporation, Corporate Technology, 300 Constitution Drive, Menlo Park, CA 94025, USA.
†To whom correspondence should be addressed.

When the number of ZnA_2 layers is reduced from seven to three, the easily visible ordering in Fig. 1A is reduced, although the long-range orientation of the molecular rows is still clearly visible (Fig. 1C). The 2D FT (Fig. 1D) shows that the lattice reflections are diffuse, in contrast to the sharp reflections in Fig. 1B. Qualitatively, the sharp reflections of Fig. 1B correspond to long-range positional order in the seven-layer film, and the diffuse reflections of Fig. 1D correspond to short-range positional order in the trilayer film. The lattice repeats—0.48 ± 0.01 nm by 0.57 ± 0.01 nm, with an angle of 53° ± 1° between them—are nearly identical to those for films of seven or more layers. The resulting area per molecule is 0.22 nm^2. The lattice symmetry and spacing and the measured bilayer thickness of 4.6 ± 0.2 nm are consistent with a 30° tilted hexagonal lattice as in the films of seven or more layers. Although the broadened reflections increase the relative error of the lattice parameters, the trilayers appear to have the same structure and interfacial density as the seven-layer films. Hence, the change in order as the number of layers is increased occurs at constant in-plane density. Although the positional order has decreased, long-range bond-orientational order is still present, as can be seen from the distinct intensity modulations in the azimuthal direction (Fig. 1D). An absence of bond-orientational order would produce a continuous ring of intensity in the FT (*16–20*).

However, we cannot immediately ascribe the diffuse spots in Fig. 1D to lack of positional order, as poor tips or image drift can lead to poor images and FTs (*10*). To confirm that the lack of order was inherent to the films, we obtained 30 to 40 drift-free images from two independent samples, using five to seven different tips per sample. The results from all tips and samples were indistinguishable. Five-layer films were qualitatively similar to the three-layer films. From these results, we conclude that monolayer films are liquid-like with short-range positional and orientational order, three- and five-layer films are hexatic with short-range positional and long-range bond-orientational order, and films of seven or more layers are crystalline with long-range positional and bond-orientational order.

To quantify the difference in positional order between the three- and seven-layer films, we present in Fig. 2, A and C, the autocorrelation function of a 10 nm by 10 nm area of the images in Fig. 1, A and C. Figure 2B, a profile along the line shown in Fig. 2A, shows that the oscillations in the autocorrelation function of the seven-layer film extend well beyond the image size; this finding implies long-range positional order. Figure 2D, a profile along the line shown in Fig. 2B, shows that positional correlations in the three-layer film decay in less than five lattice repeats. This result suggests that the distance between dislocations, which is related to the decay length of the autocorrelation function (*19*), is about five lattice repeats in the three-layer film and more than 30 lattice repeats in the seven-layer film. Similar order-of-magnitude increases in the dislocation density were observed in the transition from crystal to hexatic phase in 2D colloidal suspensions (*19*). Identifying individual dislocations in Fig. 1C is problematic because the distortions in the lattice, resulting from the high defect density, make it difficult to assign a particular site of lattice disorder to an individual dislocation.

To confirm that the bond-orientational order was long-range, we examined four distinct areas of a trilayer film that were separated by roughly 400 nm (the four corners of Fig. 3). The poor ordering in the trilayer films could be a result of randomly oriented nanometer-sized microcrystals. Over a sufficiently large region, any preferred orientation of such microcrystals is

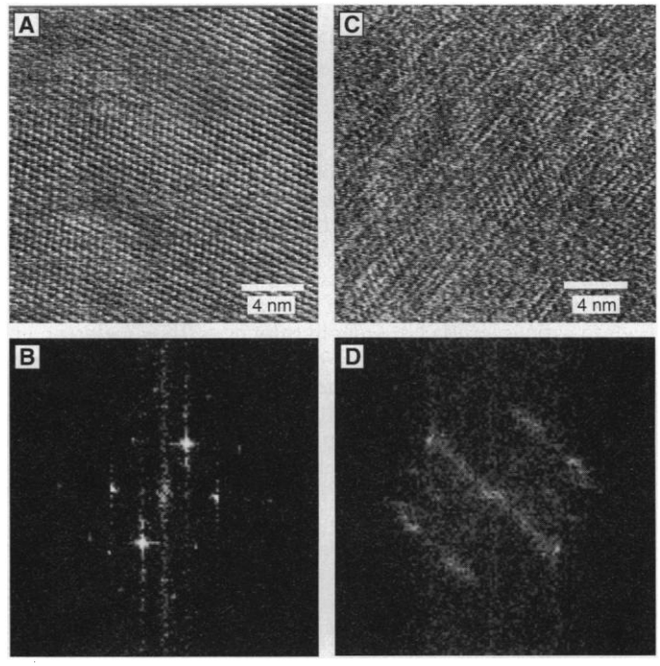

Fig. 1. Unprocessed molecular-resolution images and FTs of LB films of ZnA_2 on mica. No difference was found if the films were deposited on amorphous oxidized Si. (**A**) A 20 nm by 20 nm image of a seven-layer ZnA_2 film showing a defect-free molecular-resolution lattice. (**B**) The 2D FT of (A). The sharp, symmetric reflections are indicative of long-range positional and orientational order in the films. The vertical and horizontal streaks in the FTs are the result of noise from the raster pattern of the AFM. (**C**) A 20 nm by 20 nm image of the ZnA_2 trilayer showing the three sets of lattice rows. Compare the highly defective structure of this trilayer film to that of (A). (**D**) The 2D FT of (C). Note the broad, arclike reflections indicative of long-range orientational order but short-range positional order. The lattice parameters, symmetry, and area per molecule are the same as in the seven-layer films.

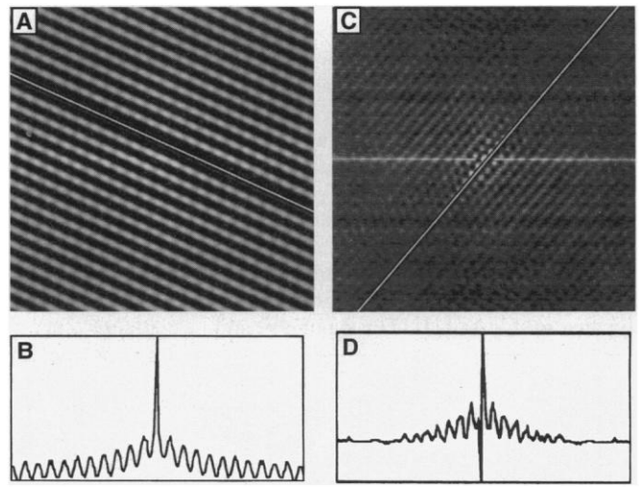

Fig. 2. (**A**) Autocorrelation function of a 10 nm by 10 nm section of Fig. 1A. (**B**) Profile plot of the line shown in the autocorrelation function in (A). The regular oscillations in the autocorrelation function extend well beyond the image size. This long-range positional order is in clear contrast to the short-range positional order of the trilayer. (**C**) Autocorrelation function of a portion of the image shown in Fig. 1C. (**D**) Profile plot of the line shown in the autocorrelation function in (C). The oscillations in the autocorrelation function die out over three to five lattice repeats, indicating short-range positional order.

lost. However, in the three-layer films, the orientational order is preserved over distances at least 100 times the positional order, consistent with a hexatic phase. The composite of the four FTs (center of Fig. 3) is qualitatively the same as any of the individual FTs, hence the orientation and short-range positional order are the same throughout the hexatic domain.

The effects of the substrate must be of a rather specific form in order for this liquid-to-hexatic-to-crystal sequence to occur as the number of layers increases. Kosterlitz and Thouless proposed that a lattice could continuously disorder or melt, with the disorder driven by the unbinding of thermally generated dislocations that destroy translational order (*16*). However, Halperin and Nelson (*17*) pointed out that long-range bond-orientational order could persist in two dimensions even in the absence of translational order. First, thermally generated dislocation pairs unbind, resulting in a continuous transition from a crystalline state to an intermediate hexatic phase that has an algebraic decay of orientational order but an exponential decay of translational order. The system subsequently makes another transition, typically induced by a further change of temperature or concentration, from the hexatic phase into a liquid with exponential decay of orientational and translational order as the dislocations unbind into pairs of disclinations (*17*). Equilibrium hexatic phases were first identified in smectic liquid crystals by x-ray and electron diffraction (*20*, *21*). Hexatic phases have also been inferred from stripe and star textures in thin smectic films (*22*) and Langmuir monolayers (*23*) and from x-ray diffraction (*24*) of Langmuir monolayers. Two-dimensional colloidal suspensions of charged polymer spheres in aqueous solution also show a hexatic phase, but with concentration rather than temperature being the control variable (*19*).

A second type of hexatic ordering, which is likely more relevant here, is induced by unbound dislocations that are pinned at lattice defects such as impurities or vacancies, or at an incommensurate or amorphous substrate (*25*). These quenched or athermal defects act similarly to the thermally generated defects in the equilibrium hexatic phase. These "hexatic glasses" have been observed in 2D alloys of hard spheres (*25*), in incommensurate charge density wave lattices (*26*), and in the Abrikosov flux lattices of superconductors with high superconducting transition temperatures (T_c) (*27*) and are ascribed to the pinning or quenching of dislocations by impurities (*28*, *29*). However, in thick ZnA_2 LB films [and generally in all thick LB films of fatty acids that we have examined (*1*)], there are very few dislocations, vacancies, or impurities in carefully prepared films (see Fig. 1, A and B). This observation, combined with the evolution in order as the number of layers is increased, suggests that the source of the defects is the substrate. This hypothesis requires that there exist positional correlations between the layers in the LB film, as well as within the layers; that is, the film is actually a 3D crystal. Although it is difficult to show this directly for the ZnA_2 films studied here, positional correlations between layers have been shown in similar LB films by AFM (*3*) and by x-ray diffraction (*30*).

Dislocations cannot terminate within a layer but rather must be part of a complete line or a half-loop with both ends anchored at sites on the substrate. (Dislocation half-loops that originate at the free surface should anneal quickly, as there is nothing to pin the dislocation.) The energy of these defects should scale with their length, so the number of dislocations should decrease as the films get thicker, and the influence of the substrate should diminish as the number of layers increases. There is likely a healing thickness that allows the perfect crystal to recover from the dislocations induced by the disordered or incommensurate substrate. The healing thickness, given by a typical dislocation loop size, is likely a function of the roughness of the substrate and the chemical nature of the substrate and LB film. Only when the film is thinner than this healing thickness can dislocation lines traverse the film and end at the free surface, where they can disrupt the positional order of the lattice and be visualized by an AFM. A similar argument can be made for disclination loops; the difference in the extent of positional and orientational order we observed in the three- and five-layer films suggests that in ZnA_2 the healing thickness for disclinations is much less than for the dislocation lines. The dislocation and disclination healing thicknesses must be roughly equal in CdA_2 and most other fatty acid films, because these films exhibit a direct transition from liquid-like monolayer to crystalline trilayer (*1*). The difference in molecular cohesion in the less densely packed ZnA_2 films may be the cause of the difference in healing thicknesses in these films.

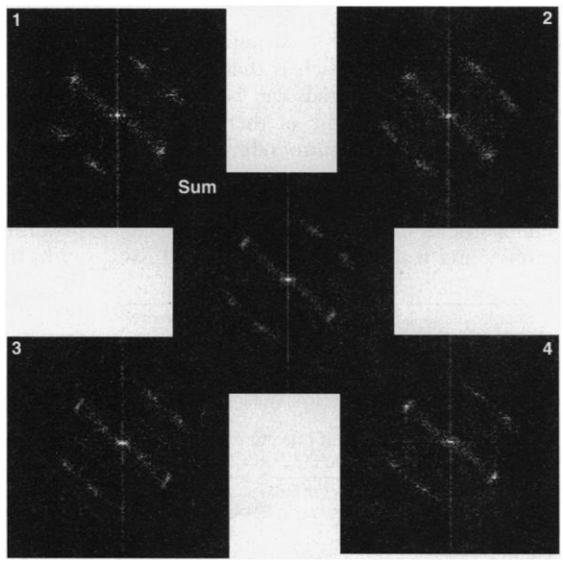

Fig. 3. Two-dimensional FTs of four independent regions (separated by about 400 nm) of the trilayer ZnA_2 film on mica, shown at the corners of the square. The composite FT, which results from the overlaying of all four independent FTs, is shown in the middle. There is no qualitative change in the FTs, especially in regard to the orientation of the reflections, between the four individual regions and the composite FT. Thus, the bond orientation is preserved over domains of micrometer extent, in comparison to the nanometer extent of positional order (see Fig. 2).

REFERENCES AND NOTES

1. J. A. Zasadzinski, R. Viswanathan, L. Madsen, J. Garnaes, D. K. Schwartz, *Science* **263**, 1726 (1994).
2. A. Bonnerot, P. A. Chollet, H. Frisby, M. Hoclet, *Chem. Phys.* **97**, 365 (1985); F. Kimura, J. Umemura, T. Takenaka, *Langmuir* **2**, 96 (1986).
3. R. Viswanathan, J. A. Zasadzinski, D. K. Schwartz, *Science* **261**, 449 (1993).
4. D. K. Schwartz, J. Garnaes, R. Viswanathan, J. A. Zasadzinski, *ibid.* **257**, 508 (1992); D. K. Schwartz, R. Viswanathan, J. A. Zasadzinski, *J. Am. Chem. Soc.* **115**, 7374 (1993); *Phys. Rev. Lett.* **70**, 1267 (1993); *Langmuir* **9**, 1384 (1993); R. Viswanathan, J. A. Zasadzinski, D. K. Schwartz, *Nature* **368**, 440 (1994).
5. G. Ungar, *J. Phys. Chem.* **87**, 689 (1983).
6. E. B. Sirota, H. E. King Jr., D. M. Singer, H. S. Shao, *J. Chem. Phys.* **98**, 5809 (1993); E. B. Sirota, H. E. King Jr., G. J. Hughes, W. K. Wan, *Phys. Rev. Lett.* **68**, 492 (1992).
7. G. Binnig, C. F. Quate, Ch. Gerber, *Phys. Rev. Lett.* **56**, 930 (1986).
8. O. Marti *et al.*, *Science* **239**, 50 (1988); M. Egger *et al.*, *J. Struct. Biol.* **103**, 89 (1990); E. Meyer *et al.*, *Nature* **349**, 398 (1991); C. J. Eckhardt *et al.*, *ibid.* **362**, 614 (1993); J. Frommer, *Angew. Chem. Int. Ed. Engl.* **31**, 1298 (1992); J. Y. Josefowicz *et al.*, *Science* **260**, 323 (1993).
9. J. Garnaes, D. K. Schwartz, R. Viswanathan, J. A. Zasadzinski, *Nature* **357**, 54 (1992); L. Bourdieu, P. Silberzan, D. Chatenay, *Phys. Rev. Lett.* **67**, 2029 (1991).
10. D. K. Schwartz *et al.*, *Phys. Rev. E* **47**, 452 (1993).
11. It has been claimed that atomic resolution of lattice defects is only possible for forces of 10^{-10} N or less; see F. Ohnesorge and G. Binnig, *Science* **260**, 1451 (1993).
12. Arachidic acid [$CH_3(CH_2)_{19}COOH$, Aldrich, 99%] (1.7 mg/ml) was spread from chloroform (Fisher

Spectranalyzed) solution onto an aqueous [water from a Milli-Q (Millipore Corporation, Bedford, MA) system was used] subphase in a commercial NIMA (Warwick Science Park, Coventry, England) trough. The subphase water included 5×10^{-4} M $ZnCl_2$ (Aldrich, 99.99%) and was adjusted to a pH of 6.5 to 7 by addition of NaOH (Aldrich, 99%). Substrates were freshly cleaved mica or polished Si wafers (Semiconductor Processing, Boston, MA) [orientation (100), 3 ohm-cm, *n*-type with a root mean square roughness of ~3 Å as measured by an AFM]. Before deposition, the Si wafers were cleaned in a hot solution of H_2O_2-H_2SO_4 (3:7 ratio) to remove any organic contaminants while leaving the amorphous native oxide intact, then stored in clean water until use. The mica substrates were cleaned by continuous rinsing with ethanol for 5 min. After removal from the ethanol bath, we cleaved the mica, using ordinary adhesive tape, and inserted it into the subphase. LB films were deposited at a surface pressure of 30 mN/m at 22.0° ± 0.5°C.

13. Resolution in our AFM images was assessed as follows. We evaluated the degree of drift in the image by comparing FTs of images scanned in opposite directions (up and down). The initial variations between spot positions from up and down scans were often as large as 0.1 nm in position and 3° in angle. However, after scanning times on a single area ranging from 0.5 to 2 hours, Fourier spots from the two scan directions were in the same location within our ability to measure them, given the digitization of the data on the display (0.01 nm, 0.5°). No damage was done to the sample even after hours of continuous imaging. We examined each sample with several AFM tips to eliminate any systematic errors arising from multiple or asymmetric tips. Typical forces were estimated to be 10^{-8} N. This protocol was essential to ensure that the disorder present in images of the hexatic films was a result of the film disorder and not thermal drift or hysteresis in the piezo drivers. A detailed discussion of AFM calibration, errors, and reproducibility is presented elsewhere (*10*).
14. The approximate tilt angle that maximizes close packing for an all-*trans* alkane chain is $\tan \theta = R/D$, where R is the next nearest carbon spacing in the all-*trans* chain, 2.5 to 2.6 Å, and D is the separation between molecules, about 4.7 to 4.8 Å for nearest neighbors in this lattice. For nearest neighbors, the first tilt is ≈28°, which is consistent with the tilt angle suggested by the ratio of the two lattice vectors, $\cos \theta = 0.48/0.56$, about 31°, and the ratio of the measured bilayer thickness of 4.7 nm to the extended length of an arachidic acid bilayer of 5.5 nm, or $\cos \theta = 4.7/5.5$, about 30°.
15. A. I. Kitaigorodskii, *Organic Chemical Crystallography* (Consultant Bureau, New York, 1961).
16. J. M. Kosterlitz and D. J. Thouless, *J. Phys. C* **5**, L124 (1972); *ibid.* **6**, 1181 (1973).
17. B. I. Halperin and D. R. Nelson, *Phys. Rev. Lett.* **41**, 121 (1978); *ibid.*, p. 519; D. R. Nelson and B. I. Halperin, *Phys. Rev. B* **19**, 2457 (1979).
18. For an excellent summary of the theoretical and experimental work in this area, see K. J. Strandburg, Ed., *Bond Orientational Order in Condensed Matter Systems* (Springer-Verlag, New York, 1992).
19. C. A. Murray and D. H. Van Winkle, *Phys. Rev. Lett.* **58**, 1200 (1987); C. A. Murray and R. A. Wenk, *ibid.* **62**, 1643 (1989).
20. R. J. Birgeneau and J. D. Litster, *J. Phys. (Paris) Lett.* **39**, L-399 (1978); J. D. Brock *et al.*, *Phys. Rev. Lett.* **57**, 98 (1986).
21. R. Pindak, D. E. Moncton, S. C. Davey, J. W. Goodby, *Phys. Rev. Lett.* **46**, 1135 (1981); M. Cheng, J. T. Ho, S. W. Hui, R. Pindak, *ibid.* **59**, 1112 (1987).
22. J. Maclennan and M. Seul, *ibid.* **69**, 2082 (1992).
23. X. Qiu *et al.*, *ibid.* **67**, 703 (1991); J. V. Selinger, Z.-G. Wang, R. F. Bruinsma, C. M. Knobler, *ibid.* **70**, 1139 (1993).
24. K. Kjaer *et al.*, *ibid.* **58**, 2224 (1987); C. A. Helm, H. Mohwald, K. Kjaer, J. Als-Nielsen, *Biophys. J.* **52**, 381 (1987).
25. D. R. Nelson, M. Rubenstein, F. Spaepen, *Philos. Mag. A* **46**, 105 (1982).
26. H. Dai, H. Chen, C. M. Lieber, *Phys. Rev. Lett.* **66**, 3183 (1991); H. Dai and C. M. Lieber, *ibid.* **69**, 1576 (1992); *J. Phys. Chem.* **97**, 2362 (1993).
27. D. J. Bishop, P. L. Gammel, D. A. Huse, C. A. Murray, *Science* **255**, 165 (1992); C. A. Murray *et al.*, *Phys. Rev. Lett.* **64**, 2312 (1990).
28. E. M. Chudnovsky, *Phys. Rev. B* **40**, 11355 (1989).
29. M. C. Marchetti and D. R. Nelson, *ibid.* **41**, 1910 (1990).
30. M. Prakash, J. B. Peng, J. B. Ketterson, P. Dutta, *Chem. Phys. Lett.* **128**, 354 (1986).
31. We thank D. R. Nelson for his suggestion that the substrate could be the source of defects and C. Knobler, E. Sirota, and R. Pindak for discussions on Langmuir films, rotator phases, and hexatics. We thank C. Jeppeson and J. Woodward for help with the image analysis software and F. Grunfeld for technical assistance with the LB trough. This work was supported by Office of Naval Research grant N00014-90-J-1551, NSF grant CTS-9305868, NIH grants GM47334 and HL51177, and the Materials Research Laboratories (MRL) Central Facilities supported by NSF under award DMR-9123048.

1 February 1995; accepted 27 April 1995

Synthesis and Structure of an Iron(III) Sulfide–Ferritin Bioinorganic Nanocomposite

Trevor Douglas,* Dominic P. E. Dickson, Steven Betteridge, John Charnock, C. David Garner, Stephen Mann†

Amorphous iron sulfide minerals containing either 500 or 3000 iron atoms in each cluster have been synthesized in situ within the nanodimensional cavity of horse spleen ferritin. Iron-57 Mössbauer spectroscopy indicated that most of the iron atoms in the 3000–iron atom cores are trivalent, whereas in the 500–iron atom clusters, approximately 50 percent of the iron atoms are Fe(III), with the remaining atoms having an effective oxidation state of about +2.5. Iron K-edge extended x-ray absorption fine structure data for the 500–iron atom nanocomposite are consistent with a disordered array of edge-shared FeS_4 tetrahedra, connected by $Fe(S)_2Fe$ bridges with bond lengths similar to those of the cubane-type motif of iron-sulfur clusters. The approach used here for the controlled synthesis of bioinorganic nanocomposites could be useful for the nanoscale engineering of dispersed materials with biocompatible and bioactive properties.

The nanoscale synthesis of inorganic particles is currently of great interest in materials chemistry (*1*). One possible route to the preparation of such materials involves the use of preorganized biomolecular architectures as chemically and spatially confined environments for the construction of inorganic clusters and nanoparticles (*2*). The 8-nm polypeptide cage of the Fe storage protein ferritin has been used to prepare nanocomposites containing pure phases of magnetite [Fe_3O_4 (magnetoferritin)] (*3*), amorphous uranium oxide (*4*), and amorphous MnOOH (*4*, *5*). An advantage of this biomimetic approach is that the inorganic nanoscale materials can be rendered biocompatible by virtue of their intimate association with the surrounding polypeptide assembly. Thus, if appropriate synthetic routes could be developed, bioinorganic nanoparticles might be useful as biological sensors and markers, drug carriers, and diagnostic and bioactive agents. For example, magnetoferritin shows potential as a contrast agent for magnetic resonance imaging of tissue (*6*) and uranium oxide–loaded ferritin could have use in neutron-capture therapy (*7*).

The synthesis of metal sulfides within ferritin could be a feasible route to the controlled construction of semiconductor and nonstoichiometric particles with technological, and perhaps biological, importance. The transformation of the hydrated iron(III) oxide [ferrihydrite ($FeOOH{\cdot}nH_2O$)] core of native ferritin to an iron sulfide has been investigated under alkaline (pH 8.9) reaction conditions (*4*, *8*). Electron diffraction (*4*) and ^{57}Fe Mössbauer spectroscopy (*8*) indicated that the product consisted of a thin surface coating of amorphous iron(II) sulfide on an essentially unmodified crystalline ferrihydrite core.

In this report, we describe a method for the in situ synthesis of iron sulfides in ferritin that results in the complete transformation of native or reconstituted iron oxide cores. An approach involving demetallation, reconstitution, and chemical reaction allows control over the particle size. The reaction product is a highly unusual amorphous sulfide consisting predominantly of trivalent Fe; insight into the local structure has been gained by extended x-ray absorption fine structure (EXAFS) analysis, a

T. Douglas and S. Mann, School of Chemistry, University of Bath, Bath BA2 7AY, UK.
D. P. E. Dickson and S. Betteridge, Department of Physics, University of Liverpool, Liverpool L69 3BX, UK.
J. Charnock, Daresbury Laboratory, Warrington, Cheshire WA4 4AD, UK.
C. D. Garner, Department of Chemistry, University of Manchester, Manchester M13 9PL, UK.

*Present address: Department of Biological and Physical Sciences, Montana State University, Billings, MT 58101, USA.
†To whom correspondence should be addressed.